Title: Frictional weakening leads to unconventional singularities during laboratory earthquakes

Authors: F. Paglialunga[1]*, F. Passelègue[1], M. Lebihain[1,2], M. Violay[1]

Affiliations:

[1]École Polytechnique Fédérale de Lausanne, LEMR, Lausanne, Switzerland

[2]École Nationale des Ponts et Chaussées, Laboratoire Navier, Champs-sur-Marne, France

*Corresponding author. Email: federica.paglialunga@epfl.ch

Abstract: Earthquakes (i.e. frictional ruptures) are commonly described by singular solutions of shear cracks motions, originally derived to describe brittle failure of materials. Such singular solutions are controlled by a square root singularity and imply a scale-independent edge-localized energy balance, in disagreement with recent observations of large-scale thermal weakening. This continuous weakening is expected to deviate the singularity order from the square root singularity, modifying the dynamics around the rupture tip and leading to a scale dependent energy release rate. Here, we present the first experimental evidence of frictional rupture driven by enhanced thermal weakening, whose rupture fronts present unconventional singularity orders and slip-dependent breakdown work. This work strengthens the idea of a presumable unconventional nature of earthquakes, and highlights the difficulty in a priori estimating the energy balance controlling the extension and the rupture velocity of the seismic rupture.

Plain Language Summary: When an earthquake nucleates in the earth crust, the potential energy accumulated during the inter-seismic period is released into breakdown work, heat energy and radiated energy. Often the breakdown work is considered a seismological equivalent of the fracture energy. However, discrepancies related to the definition of the two are not yet fully solved. To this end, we reproduced frictional ruptures in the laboratory to study the relationship between these two energies. A dual strength weakening is observed, reflected in a scale dependent evolution of breakdown work with fault' slip, contrarily to fracture energy which is, by definition, scale independent. This behavior shows to be probably caused by thermal weakening (i.e. flash heating) activated during slip and to be well described by the recently developed unconventional theory of frictional ruptures (i.e. rupture driven by a non-square root singularity). Importantly, these results highlight, from an experimental point of view, the presumable unconventional nature of earthquakes, solving the discrepancies between breakdown work and fracture energy. Moreover, it suggests that an analysis of the propagating rupture in the framework of linear elastic fracture mechanics could prove to be not always sufficiently exhaustive when frictional weakenings occur, as it is expected along crustal faults.

Introduction:

Frictional rupture phenomena, including natural earthquakes, are commonly described by regular singular solutions of shear crack motions (Freund, 1990; Palmer and Rice, 1973; Rice, 1980). For such cracks, the stress field at the rupture tip is described by a square root singularity ($\xi = -0.5$) and the energy balance condition equates the energy release rate to a constant value of fracture energy (G_c). This was confirmed by experimental observations, where the onset of frictional sliding, the evolution of the rupture speed and the rupture length were predicted by Linear Elastic Fracture Mechanics (LEFM) (Bayart, Svetlizky, and Fineberg 2016a; Kammer and Mclaskey 2019; Svetlizky and Fineberg 2014; Xu, Fukuyama, and Yamashita 2019).

However, recent works highlighted that rocks and faults are likely to weaken or strengthen during seismic slip due to (i) velocity and slip dependencies (Marone 1998), (ii) activation of thermal weakening processes (Hirose and Shimamoto 2005; Rice 2006; Toro et al. 2011), (iii) dilatancy inducing fluid pressure changes (Brantut 2020; Rice and Rudnicki 1979; Segall et al. 2010), and (iv) stress barrier and frictional heterogeneities (Das and Aki 1977). As a result, the local residual stress behind the rupture tip could change drastically during seismic slip, continuously modifying the tip-localized energy balance (G=G_c) and making the complete breakdown work (W_{bd}) (Tinti, Spudich, and Cocco 2005), energy term including all on-fault dissipative processes, a slip dependent quantity (Abercrombie and Rice 2005; Lambert and Lapusta 2020). This could eventually lead to stress and displacement fields around the rupture tip governed by unconventional singularities order, that deviate from LEFM ($\xi \neq -0.5$) (Brantut and Viesca 2017; Brener and Bouchbinder 2021a; Garagash, Detournay, and Adachi 2011; Viesca and Garagash 2015), raising the question of the applicability of such framework in analyzing and predicting earthquake motions. Indeed, altough recent study showed how the observed scaling of W_{bd} with slip could be explained by a stress overshoot without the need of an on-fault frictional weakening (Ke, McLaskey, and Kammer 2021), given some evidence of fault's weakening during natural earthquakes (Di Toro et al. 2006), it remains reasonable to think that natural ruptures could present stress fields controlled by unconventional singularities, that cannot be described and analyzed using standard LEFM. For instance, recent works already highlighted that the weakening occurring far away from the rupture tip can contribute, for sufficiently large systems, to the rupture dynamics (Barras et al. 2020; Garagash 2021). However, so far, the occurrence of such unconventional singularities has not been measured at the laboratory scale during frictional ruptures. Here, we

present the first experimental evidence of strain and stress perturbation controlled by unconventional singularities associated to velocity-dependent frictional weakening.

Methods and Results:

We performed stick-slip experiments on PMMA samples under normal stress ranging from 1 to 4 MPa. Strain gages rosettes, located at 1 mm from the frictional interface, were used to analyze each rupture event, studying the evolution of shear stress, slip velocity and material displacement as function of the distance from the rupture tip (Fig.1) (see supplementary material). In all events studied, local shear stress evolution exhibited an increase ahead of the rupture tip followed by a first significant decrease within the first micrometers of slip and a second mild one within larger distances (Fig.1a). A rapid increase of slip velocity was observed concurrent with the passage of the rupture front, followed by a slow decay occurring with distance from the rupture tip. The peak slip velocity (V_{max}) showed a clear dependence with estimated rupture speed (C_f), ~0.08 m/s for C_f of ~220 m/s up to 0.8 m/s for C_f of ~840 m/s (Fig.1b). The evolution of material displacement (u_x) showed profiles coherent with previous works (Berman, Cohen, and Fineberg 2020), presenting values close to 0 m ahead of the rupture tip and a sharp increase behind it (Fig.1c), with final displacements ranging between $3.9\ 10^{-6}$ and $28\ 10^{-6}$ m. The estimate of the latter results from two main hypothesis: (i) the material displacement measured through the strain gauge at 1 mm from the fault is comparable to the one occurring on the fault, (ii) the fault's displacement is computed as twice the local displacement assuming a symmetric displacement distribution. Note that the following interpretation is independent of the second hypothesis.

Subsequently, the interface' strength weakening was analyzed through the evolution of the local shear stress with fault's displacement (D). The fault's weakening presents a first sharp decrease of shear stress occurring within the first microns of slip, followed by a milder decrease occurring within a larger amount of slip (Fig.2a). The increasing breakdown work was computed as $W_{bd} = \int_0^D (\tau - \tau(D))\, dD$. Its evolution with slip showed a first increase described by a slope close to 1:2 and a subsequent increase described by a slope of ~1:0.6 (Fig.2b). While the first stage of the breakdown work evolution can be explained by a slip weakening behavior of the fault, the subsequent increase of breakdown work with slip (power law of ~1:0.6) is unexpected from the conventional theory of LEFM. In the latter, a plateau emerging right after the first stage is expected, indicator of a scale independent breakdown work (i.e. no additional dissipation outside of the cohesive zone), and comparable to the definition of fracture energy (G_c) (Freund 1998). This

secondary increase in W_{bd} with slip is, however, compatible with evolutions observed during high velocity frictional experiments exhibiting thermal weakening (see G Di Toro et al. 2011 for a review).

If such secondary weakening stage controlled the dynamics of the rupture, unconventional stress fields should be observed around the rupture tip as expected from theoretical studies (Brantut and Viesca 2017; Brener and Bouchbinder 2021a; Garagash et al. 2011; Viesca and Garagash 2015).

Contrarily to a propagating crack controlled by a square root singularity ($\xi = -0.5$) (Freund 1998), frictional ruptures can generate a singular field described by $\xi \neq -0.5$, due to the continuous weakening experienced by the interface behind the rupture tip. In such conditions, stress and displacement fields obey the following scaling relationships for respectively the stress (σ) and displacement (u) fields (Brener and Bouchbinder 2021a): $\sigma \approx K^{(\xi)} r^{\xi}$ and $u \approx K^{(\xi)} r^{\xi+1}/\mu$, with $K^{(\xi)}$ the ξ- generalized stress intensity factor, $= x - x_{tip}$ the distance from the rupture tip, and μ the dynamic shear modulus, leading to the following relation: $W_{bd} \sim [K^{(\xi)}]^2 \, r^{1+2\xi}/\mu$, valid for $r > x_c$ (eq.5 from (Brener and Bouchbinder 2021a)). From this relation, we can directly notice that when $\xi = -0.5$, the W_{bd} dependence on r completely vanishes, making the breakdown work independent of the distance from the rupture tip. However, this is not true when $\xi \neq -0.5$, for which W_{bd} has a direct dependence on r. Following the theory (Brener and Bouchbinder 2021a), we can define a critical fault displacement D_c for which the W_{bd} evolution with slip changes from a power law of exponent ~2 to a power law of exponent ~0.6. The value of W_{bd} reached at D_c corresponds to the fracture energy G_c, quantity expected to control the rupture propagation.

To investigate whether the prolonged fault weakening controls the rupture dynamics at the scale of our experiments, the experimental evolutions of $\Delta\varepsilon_{xy}$, $\Delta\varepsilon_{xx}$ and $u_x$were compared to the predictions derived from the kinematic field controlled by an unconventional singularity order. Unlike LEFM, in which the shear stress acting on the crack's interface is assumed to vanish (or to reach a residual constant value outside of the cohesive zone), allowing the assumption of traction-free condition which is satisfied considering a singularity $\xi = -0.5$, frictional ruptures are expected to be controlled by an unconventional singularity when the shear stress changes as function of the slip velocity experienced.

The displacement field related to the unconventional rupture phenomenon can be predicted by (Brener and Bouchbinder 2021a):

$$u_x(r,\theta) = \frac{2K_{II}^{(\xi)}}{\mu\sqrt{2\pi}\,R(C_f)}\left[2\alpha_s r_d^{\xi+1}\,sin((\xi+1)\theta_d) - \alpha_s(1+\alpha_s^2)\,r_s^{\xi+1}\,sin((\xi+1)\theta_s)\right] \quad \text{Eq. 1}$$

$$u_y(r,\theta) = \frac{2K_{II}^{(\xi)}}{\mu\sqrt{2\pi}\,R(C_f)}\left[2\alpha_s\alpha_d r_d^{\xi+1}\,cos((\xi+1)\theta_d) - (1+\alpha_s^2)\,r_s^{\xi+1}\,cos((\xi+1)\theta_s)\right] \quad \text{Eq. 2}$$

with $K_{II}^{(\xi)} = \lim_{r\to 0}\frac{2\sqrt{2\pi}}{(\xi+1)} r^{-\xi}\tau(r,0^{\pm})$ the ξ-generalized stress intensity factor, $\alpha_d = 1-\left(\frac{C_f}{C_d}\right)^2$, $\alpha_s = 1-\left(\frac{C_f}{C_s}\right)^2$ where (C_d, C_s) are the P-wave and S-wave speed respectively, and $R = 4\,\alpha_d\alpha_s - (1+\alpha_s^2)^2$ the Rayleigh function.

As commonly adopted in fracture mechanics problems, coordinates are expressed in the polar system with (r,θ) respectively the distance from the crack tip and the angle with respect to the crack's plane. (r,θ) are corrected for the distortion produced by C_f, becoming $\theta_d = \arctan(\alpha_d\tan(\theta))$, $\theta_s = \arctan(\alpha_s\tan(\theta))$ and $r_d = r\sqrt{1-\left(\frac{C_f\sin(\theta)}{C_d}\right)^2}$, $r_s = r\sqrt{1-\left(\frac{C_f\sin(\theta)}{C_s}\right)^2}$.

To be able to compare the strain evolution observed during the experiments with the theoretical predictions coming from the unconventional theory, the stress field was derived from the elastodynamic equations assuming a steady-state rupture velocity, taking the following form:

$$\sigma_{xx}(r,\theta) = \frac{2(\xi+1)K_{II}^{(\xi)}}{\sqrt{2\pi}\,R(C_f)}\left[2\alpha_s\left(1-\alpha_s^2+2\alpha_d^2\right)r_d^{\xi}\,sin(\xi\theta_d) - 2\alpha_s(1+\alpha_s^2)r_s^{\xi}\,sin(\xi\theta_s)\right] \quad \text{Eq. 3}$$

$$\tau(r,\theta) = \frac{2(\xi+1)K_{II}^{(\xi)}}{\sqrt{2\pi}\,R(C_f)}\left[4\alpha_s\alpha_d\,r_d^{\xi}\,cos(\xi\theta_d) - (1+\alpha_s^2)^2\,r_s^{\xi}\,cos(\xi\theta_s)\right] \quad \text{Eq. 4}$$

$$\sigma_{yy}(r,\theta) = \frac{2(\xi+1)K_{II}^{(\xi)}}{\sqrt{2\pi}\,R(C_f)}\left[-2\alpha_s(1+\alpha_s^2)r_d^{\xi}\,sin(\xi\theta_d) + 2\alpha_s(1+\alpha_s^2)r_s^{\xi}\,sin(\xi\theta_s)\right] \quad \text{Eq. 5}$$

The strain and displacement fields were estimated using values of ξ computed through the evolution of the secondary increase of W_{bd} with D using: $W_{bd}(D) = G_c\left(\frac{D}{D_c}\right)^{\frac{1+2\xi}{1+\xi}}$ (Brener and Bouchbinder 2021b), and were found ranging between -0.4 and -0.2, depending on C_f and V_{max}

(Fig. 2 inset). Given the relationship linking $W_{bd}(D)$ with $K_{II}^{(\xi)}$ (eq.5 from (Brener and Bouchbinder 2021a)), the stress intensity factor was computed as: $K_{II}^{(\xi)} = \sqrt{\frac{E\, W_{bd}(D_{fin})}{(1-\nu^2)\, f_{II}(C_f)\; r^{1+2\xi}}}$ with E, ν, respectively the elastic modulus and Poisson's ratio and $f_{II}(C_f) = \frac{\alpha_s}{(1-\nu)R(C_f)} \frac{C_f^2}{C_s^2}$ the universal function of rupture speed.

The experimental data were also compared with the predictions of LEFM ($\xi = -0.5$) inverting G_c from the best possible fit of $\Delta\varepsilon_{xx}$ and $\Delta\varepsilon_{xy}$ (Svetlizky and Fineberg 2014) (Fig. 3). Note that the latter requires value of G_c not always consistent with W_{bd}. This is reflected in the accuracy with which the LEFM predictions of $\Delta\varepsilon_{xx}$ and $\Delta\varepsilon_{xy}$ describe the experimental curves. Concerning $\Delta\varepsilon_{xx}$ evolutions, LEFM predictions do not deviate excessively from the experimental curves for both events displayed in Fig.3, showing an acceptable description of the strain perturbation. In the same way, the unconventional model predictions reasonably describe $\Delta\varepsilon_{xx}$ evolutions for both events (Fig. 3b., c.), with estimated singularity order of respectively $\xi = -0.32$ and $\xi = -0.27$. However, a strong influence on the ξ values is observed in the evolutions of $\Delta\varepsilon_{xy}$. Behind the rupture tip, we can observe that for the two events, the unconventional singularity model fully describes the experimental curves, while LEFM naturally fails as it assumes a more abrupt stress drop and a constant residual stress. In particular, the more ξ deviates from -0.5, the largest the discrepancies between LEFM and the unconventional model (Fig. 3b., c.). Prediction of $\Delta\varepsilon_{xy}$ fail ahead of the rupture tip for both models, because (i) they assume the background stress equal to the residual stress far from the rupture tip, and (ii) the theoretical prediction of the stress fields ahead of the rupture tip requires an infinite fault ahead of the tip, conditions which are not respected in our experimental configurations.

Overall, the unconventional singularity model provides convincing predictions for a wide variety of dynamic quantities ($\Delta\varepsilon_{xy}$, $\Delta\varepsilon_{xx}$ and u_x) from the sole evolution of the breakdown work with slip. Note that the estimated values of ξ are comprised in the range $-0.5 < \xi < 0$, characteristic of a velocity-strengthening behavior (Brener and Bouchbinder 2021a), confirmed by the frictional response of the fault far from the rupture tip (Fig. 3a).

Discussion

These results show first evidence of unconventional stress fields during the dynamic propagation of laboratory frictional rupture, caused by a continuous stress weakening behind the rupture tip.

The observed unconventional singularity orders could emerge, among others, from frictional weakening mechanisms such as; thermal activation (Bar-sinai et al. 2014), viscous-friction (Brener and Marchenko 2002), powder lubrication (Reches and Lockner 2010), flash heating (Brantut and Viesca 2017; Rice 2006), thermal pressurization (Rice 2006; Viesca and Garagash 2015). Among these, flash heating has been shown to be activated under similar experimental conditions (Rubino, Rosakis, and Lapusta 2017), thus could be the best candidate to explain the unconventional stress fields observed in our experiments. While flash heating is expected to induce at a first order a 1/V dependence in friction (i.e. velocity weakening frictional behavior, in disagreement with the ξ evolution observe in our experiments), the apparent velocity strengthening behavior observed in our experiments is expected to emerge solely from the coupling between elastodynamics and frictional motions (Rosakis, Rubino, and Lapusta 2020).

Flash heating is activated when the fault slip velocity becomes higher than a critical weakening slip velocity (V_w), causing mechanical degradation of contact asperities during their lifetime (Goldsby and Tullis 2011; Rice 2006). The temperature reached at the asperities was computed trough $T_{asp} = T_{amb} + \frac{1}{\rho c_p \sqrt{k\pi}} \tau_c V \sqrt{t_c}$ with T_{amb} the ambient initial temperature, τ_c the stress acting on the single asperity, t_c the lifetime of a contact, ρ the bulk density, c_p the bulk specific heat and k the thermal diffusivity. Under our experimental conditions, temperature increased with slip velocity, overpassing the melting temperature of the material ($T_{asp} > T_{melting} = 160℃$) (Fig.4b), indicating that melting of asperities probably occurred in our experiments (Rubino et al. 2017).

We compared the evolution of W_{bd} with D, normalized respectively by G_c and D_c, with asymptotic solutions for flash heating phenomena (Brantut and Viesca 2017). The evolution of W_{bd} for small slip ($D < D_c$) can be described by the asymptote derived for adiabatic conditions (Brantut and Viesca 2017):

$$W_{bd} = \rho c\,(T_m - T_{amb}) w \sqrt{2\pi} \left(\frac{D}{V\, t_w^A + D}\right)^2 \qquad \text{Eq. 6}$$

where $t_w^A = \frac{\rho C (T_m - T_f)}{\tau_a} \frac{\sqrt{2\pi} w}{V_w}$ (time required for a layer of thickness $\sqrt{2\pi} w$ to reach $T_{melting}$ (32)), w is the fault's width (assumed here as $w = 4a$ with a the asperity size) , and τ_a is a normal stress dependent contact shear stress at the origin of the change in temperature in the fault layer (Fig. 4c). In presence of gouge along the interface, τ_a will corresponds to the macroscopic shear stress

τ_0. Along bare rock interfaces, $\tau_a = \tau_c \frac{a}{\Delta L_{asp}}$, where ΔL_{asp} is the average distance between two asperities (See supplementary material for more details). Please note that this model assumes a constant V, assumption which reveals reasonable in our case, considering that the first part of the stress weakening ($D < D_c$) occurs in a very short time window, during which V can be approximated with a constant value.

For $D > D_c$, a second asymptotic solution considering the coupled elastodynamics and frictional motions of the propagating rupture can be used (Brantut and Viesca 2017):

$$W_{bd} = \tau_c \, D_w^{SP} \left(\frac{\mu \, V_w}{3\pi \, \tau_a \, C_f}\right)^{1/3} \left(\frac{D}{D_w^{SP}}\right)^{2/3} \qquad \text{Eq. 7}$$

where $D_w^{SP} = V_w \alpha \left(\frac{\rho C (T_w - T_f)}{\tau_a V_w}\right)^2$ is a characteristic slip weakening distance. Assuming our experimental estimate of C_f, this asymptote well describes the second branch of the evolution of W_{bd} with D (power law with exponent of 2/3, Fig. 4c). Such scaling is also observed at large slip for thermal pressurization in drained conditions, suggesting that such exponent is related to diffusion mechanisms regulating the weakening of faulting during seismic slip (Brantut and Viesca 2017; Viesca and Garagash 2015).

Such clear evidence of unconventional stress fields was not observed in similar experiments, for which LEFM commonly well described rupture dynamics (Bayart, Svetlizky, and Fineberg 2016b; Kammer and Mclaskey 2019; Svetlizky and Fineberg 2014). This could be ascribed to the fact that the distribution of background stress is relatively high in the present experiments. This would drive the system towards higher slip rates, and could help promoting flash heating mechanisms over rate and state friction. Moreover, the high slip rate measured near-fault enhances the activation of flash heating as previously showed. This agrees with the clear dependence of ξ values with maximum slip rate and rupture velocity observed in our events (inset Fig. 2b.): higher V_{max} are associated with ξ values which deviate from the conventional value (-0.5).

Conclusions

We showed that during laboratory earthquakes, the continuous weakening activated along the fault modifies the singularity order governing displacement and strain fields around the rupture tip, inducing a slip and scale dependent breakdown work, rather than a constant one. Moreover, this work highlights from an experimental point of view, that an analysis in the framework of linear

elastic fracture mechanics could not always be sufficiently exhaustive when frictional weakening mechanisms occur away from the rupture tip, as recently pointed out (Bayart, Svetlizky, and Fineberg 2018). Importantly, if the residual stress never reaches a steady-state value far from the rupture tip, as expected for thermal weakening processes, the singular fields will never recover the conventional square-root singularity order, independently of the rupture size. Our new results highlight the difficulty in a priori estimating the fracture energy governing the dynamics of the seismic rupture, expected to control the final rupture length (earthquake size). Our experimental results, together with the recent development of the unconventional singularity theory, open the door for a better understanding of the rupture dynamics and energy budget of natural earthquakes in the near future, through the possible evaluation of the equations of motions for unconventional rupture phenomena.

Data Availability Statement

The raw data can be found at the following address:
https://enacshare.epfl.ch/drcx43hzD2kAP5FK7B8nj

References

Abercrombie, Rachel E. and James R. Rice. 2005. "Can Observations of Earthquake Scaling Constrain Slip Weakening?" *Geophysical Journal International* 162(2):406–24.

Bar-sinai, Yohai, Robert Spatschek, Efim a Brener, and Eran Bouchbinder. 2014. "Journal of Geophysical Research : Solid Earth On the Velocity-Strengthening Behavior of Dry Friction." 2014(1):1738–48.

Barras, Fabian, Michael Aldam, Thibault Roch, Efim A. Brener, Eran Bouchbinder, and Jean-François Molinari. 2020. "The Emergence of Crack-like Behavior of Frictional Rupture: Edge Singularity and Energy Balance." *Earth and Planetary Science Letters* 531:115978.

Bayart, E., I. Svetlizky, and J. Fineberg. 2018. "Rupture Dynamics of Heterogeneous Frictional Interfaces." *Journal of Geophysical Research: Solid Earth* 123(5):3828–48.

Bayart, Elsa, Ilya Svetlizky, and Jay Fineberg. 2016a. "Fracture Mechanics Determine the Lengths of Interface Ruptures That Mediate Frictional Motion." *Nature Physics* 12(November 2015).

Bayart, Elsa, Ilya Svetlizky, and Jay Fineberg. 2016b. "Fracture Mechanics Determine the Lengths of Interface Ruptures That Mediate Frictional Motion." *Nature Physics* 12(2):166–70.

Berman, Neri, Gil Cohen, and Jay Fineberg. 2020. "Dynamics and Properties of the Cohesive Zone in Rapid Fracture and Friction." *Physical Review Letters* 125(12):125503.

Brantut, Nicolas. 2020. "Dilatancy-Induced Fluid Pressure Drop during Dynamic Rupture: Direct Experimental Evidence and Consequences for Earthquake Dynamics." *Earth and Planetary Science Letters* 538:116179.

Brantut, Nicolas and Robert C. Viesca. 2017. "The Fracture Energy of Ruptures Driven by Flash Heating." *Geophysical Research Letters* 44(13):6718–25.

Brener, E. A. and V. I. Marchenko. 2002. "Frictional Shear Cracks." *JETP Letters* 76(4):211–14.

Brener, Efim A. and Eran Bouchbinder. 2021a. "Theory of Unconventional Singularities of Frictional Shear Cracks." *Journal of the Mechanics and Physics of Solids* 153:104466.

Brener, Efim A. and Eran Bouchbinder. 2021b. "Unconventional Singularities and Energy Balance in Frictional Rupture." *Nature Communications* 12:2585.

Das, Shamita and Keiiti Aki. 1977. "Fault Plane with Barriers: A Versatile Earthquake Model." *Journal of Geophysical Research* 82(36):5658–70.

Freund, L. Ben. 1998. *Dynamic Fracture Mechanics*. Cambridge university press.

Garagash, Dmitry I. 2021. "Fracture Mechanics of Rate-and-State Faults and Fluid Injection Induced Slip." *Philosophical Transactions of the Royal Society A: Mathematical, Physical and Engineering Sciences* 379(2196).

Garagash, Dmitry I., Emmanuel Detournay, and Jose I. Adachi. 2011. "Multiscale Tip Asymptotics in Hydraulic Fracture with Leak-Off." *Journal of Fluid Mechanics* 669:260–97.

Goldsby, D. L. and T. .. Tullis. 2011. "Flash Heating Leads to Low Frictional Earthquake Slip Rates." *Science* 334(6053):216–18.

Hirose, Takehiro and Toshihiko Shimamoto. 2005. "Growth of Molten Zone as a Mechanism of Slip Weakening of Simulated Faults in Gabbro during Frictional Melting." *Journal of Geophysical Research: Solid Earth* 110(B5).

Kammer, David S. and Gregory C. Mclaskey. 2019. “Fracture Energy Estimates from Large-Scale Laboratory Earthquakes.” *Earth and Planetary Science Letters* 511:36–43.

Ke, Chun-Yu, Gregory C. McLaskey, and David S. Kammer. 2021. “Earthquake Breakdown Energy Scaling Despite Constant Fracture Energy.” 1–26.

Lambert, Valère and Nadia Lapusta. 2020. “Rupture-Dependent Breakdown Energy in Fault Models with Thermo-Hydro-Mechanical Processes.” *Solid Earth* 11(6):2283–2302.

Marone, Chris. 1998. “Laboratory-Derived Friction Laws and Their Application to Seismic Faulting.” *Annual Review of Earth and Planetary Sciences* 26:643–96.

Reches, Ze’Ev and David A. Lockner. 2010. “Fault Weakening and Earthquake Instability by Powder Lubrication.” *Nature* 467(7314):452–55.

Rice, James R. 2006. “Heating and Weakening of Faults during Earthquake Slip.” *Journal of Geophysical Research: Solid Earth* 111(5):1–29.

Rice, James R. and John W. Rudnicki. 1979. “Earthquake Precursory Effects Due to Pore Fluid Stabilization of a Weakening Fault Zone.” *Journal of Geophysical Research: Solid Earth* 84(B5):2177–93.

Rosakis, A. J., V. Rubino, and N. Lapusta. 2020. “Recent Milestones in Unraveling the Full-Field Structure of Dynamic Shear Cracks and Fault Ruptures in Real-Time : From Photoelasticity to Ultrahigh- Speed Digital Image Correlation.” *Journal of Applied Mechanics* 87(March):030801.

Rubino, V., A. J. Rosakis, and N. Lapusta. 2017. “Understanding Dynamic Friction through Spontaneously Evolving Laboratory Earthquakes.” *Nature Communications* 8(May).

Segall, Paul, Allan M. Rubin, Andrew M. Bradley, and James R. Rice. 2010. “Dilatant Strengthening as a Mechanism for Slow Slip Events.” *Journal of Geophysical Research: Solid Earth* 115(12):1–37.

Svetlizky, Ilya and Jay Fineberg. 2014. “Classical Shear Cracks Drive the Onset of Dry Frictional Motion.” *Nature* 509(7499):205–8.

Tinti, E., P. Spudich, and M. Cocco. 2005. “Earthquake Fracture Energy Inferred from Kinematic Rupture Models on Extended Faults.” *Journal of Geophysical Research: Solid Earth* 110(B12).

Toro, G. Di, R. Han, T. Hirose, N. De Paola, S. Nielsen, K. Mizoguchi, F. Ferri, M. Cocco, and T. Shimamoto. 2011. “Fault Lubrication during Earthquakes.” *Nature* 5–10.

Di Toro, Giulio, Takehiro Hirose, Stefan Nielsen, and Giorgio Pennacchioni. 2006. “Natural and Experimental Evidence During Earthquakes.” *Science* 311(5761):647–49.

Viesca, Robert C. and Dmitry I. Garagash. 2015. “Ubiquitous Weakening of Faults Due to Thermal Pressurization.” *Nature Geoscience* 8(11):875–79.

Xu, Shiqing, Eiichi Fukuyama, and Futoshi Yamashita. 2019. “Robust Estimation of Rupture Properties at Propagating Front of Laboratory Earthquakes.” *Journal of Geophysical Research* 124(1):766–88.

Fig.1

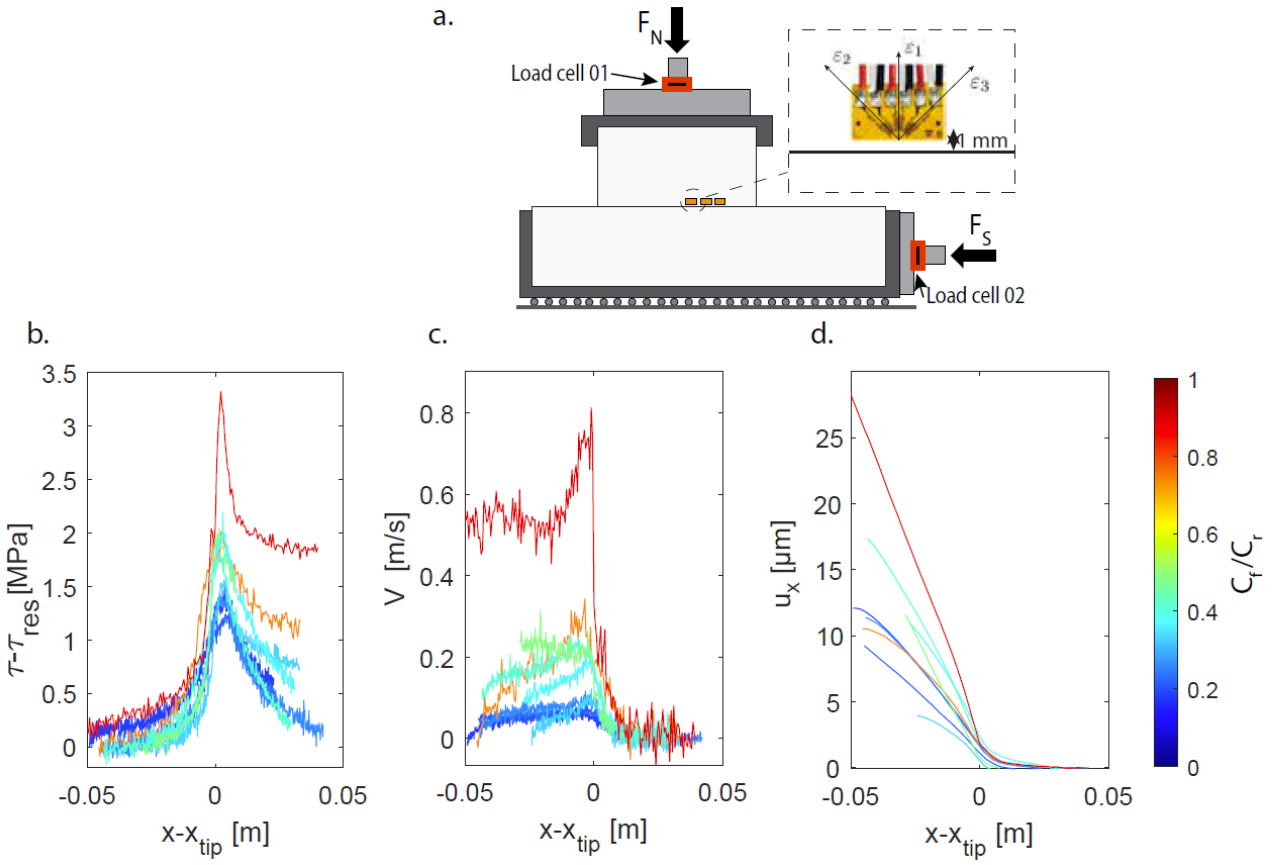

Fig. 1. Elastic fields around the rupture tip. a. Sketch of the experimental setup where the two PMMA samples are loaded to recreate the artificial fault. Evolution of **b.** shear stress computed from the measured strain (ε_{xy}), **c.** slip velocity computed from the measured strain (ε_{xx}), **d.** material displacement computed from the estimated slip velocity (for details refer to the supplementary material) for several events presenting different C_f (colorbar).

Fig.2

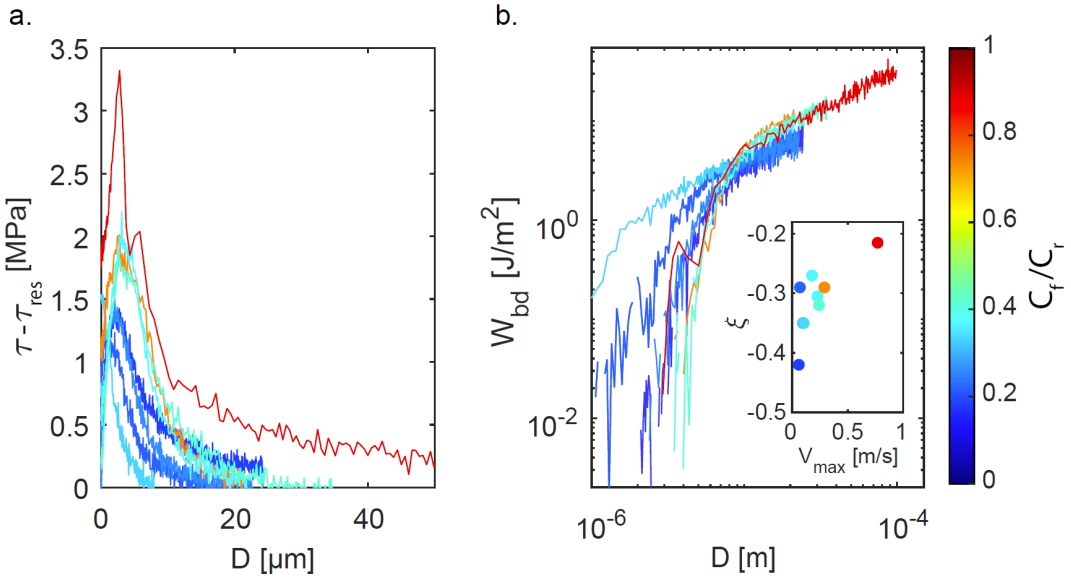

Fig. 2. Slip-dependent breakdown work and emergence of unconventional singularity. a. Evolution of $(\tau - \tau_{res})$ with D defining the fault's weakening for different events. The integration of these curves leads to the evolution of W_{bd} with D for different C_f (**b.**). In the inset the evolution of ξ with peak slip velocity (V_{max}).

Fig.3

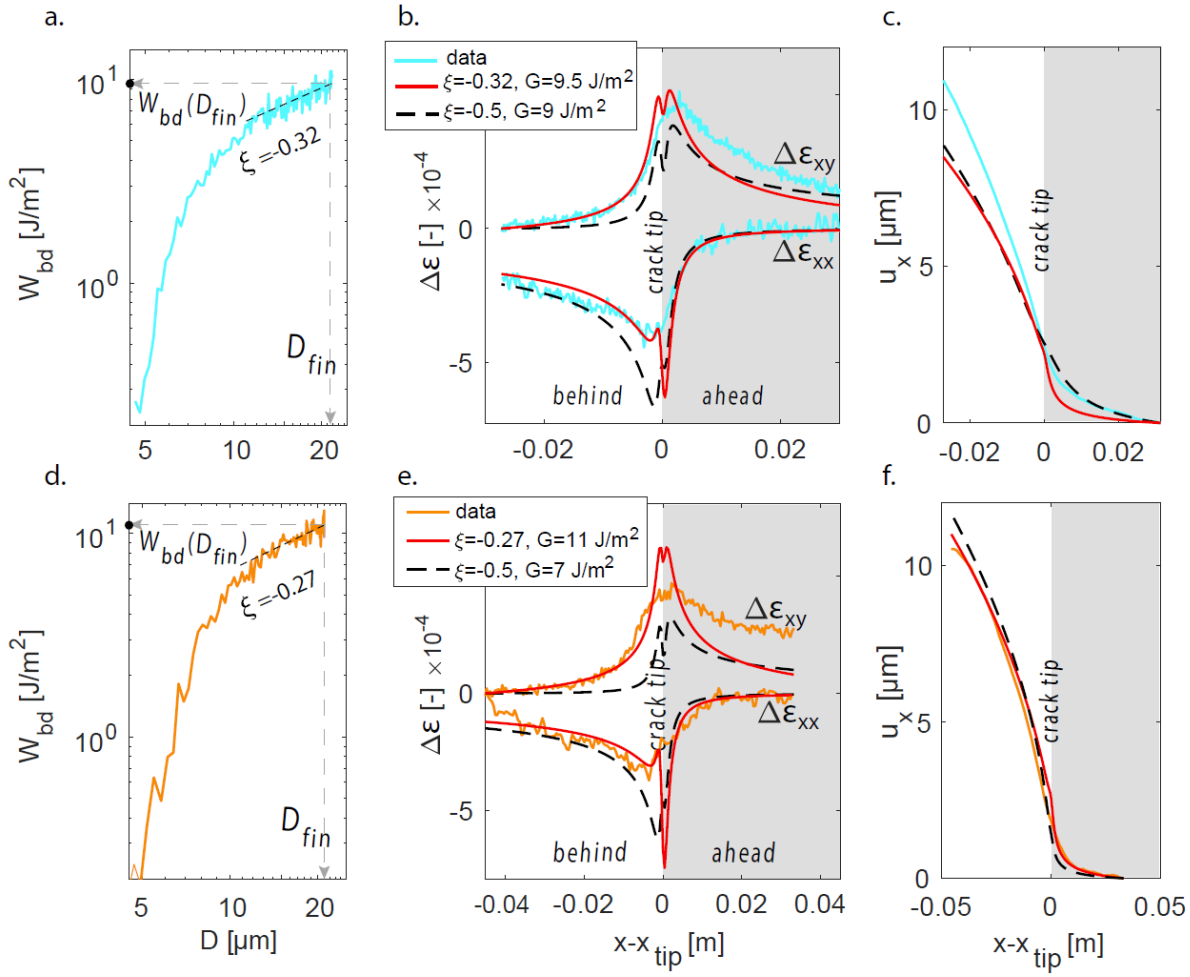

Fig. 3. Strain and displacement field described by unconventional singularity for two different events (respectively top and bottom panels). a.,d. Example of the evolution of W_{bd} with D. ξ values are retrieved through the secondary slope of W_{bd} vs D evolution (refer to main text). **b., e.** Comparison of the evolution of the measured strain perturbations $\Delta\varepsilon_{xx}$ and $\Delta\varepsilon_{xy}$ with the theoretical prediction considering: i) the estimated unconventional singularities $\xi = -0.32$ (b.) and $\xi = -0.27$ (e.) and $G = W_{bd}(D_{fin})$ (in red) and ii) the LEFM conventional singularity $\xi = -0.5$ (in dotted black) with best fit of G. **c., f.** Evolution of the material displacement (u_x) with predictions for unconventional and conventional singularity with G values respectively measured ($G = W_{bd}(D_{fin})$) and best fit. Please note that a limit of the model used for $\Delta\varepsilon_{xy}$ predictions for unconventional singularity is to assume background stress equal to residual stress. This assumption is not met in our experiments, so the reader should focus on the evolution behind the rupture tip (white area).

Fig.4

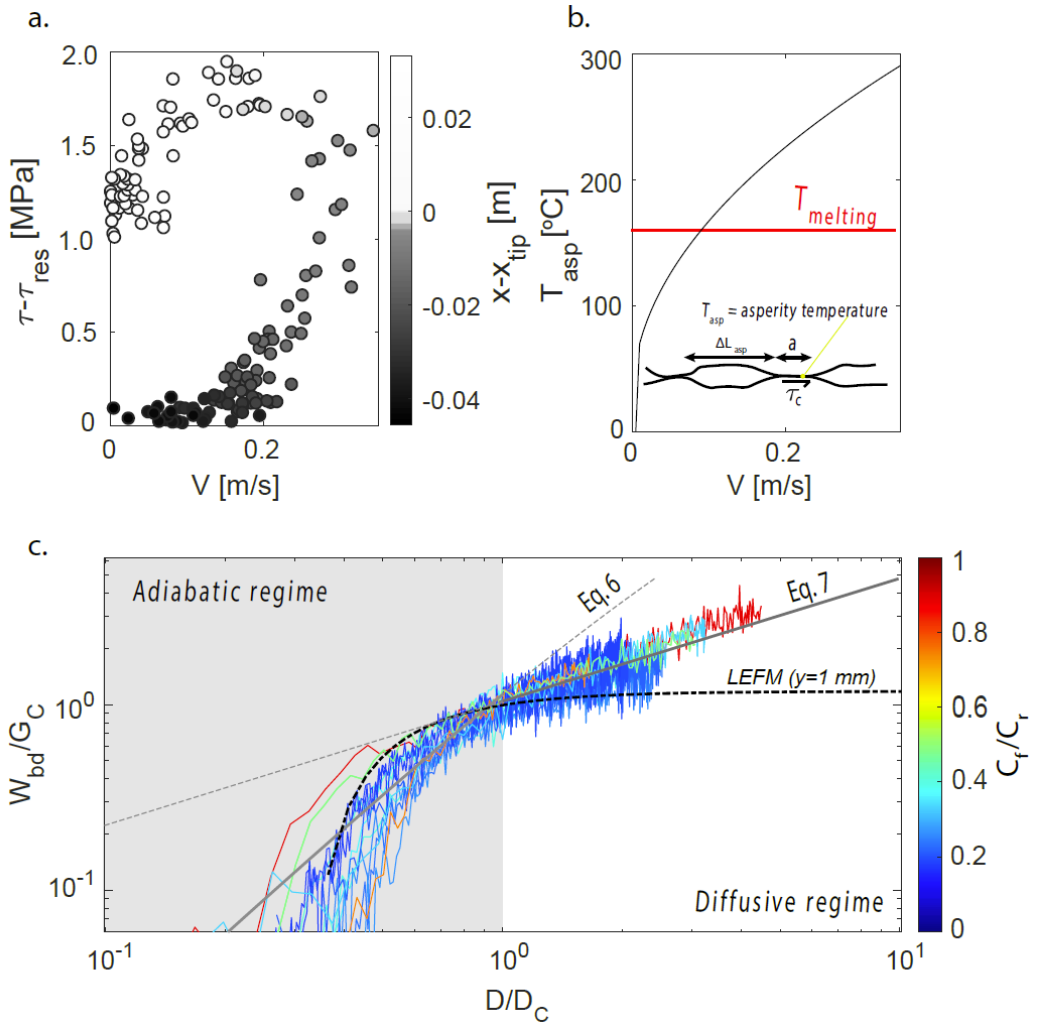

Fig. 4. Thermal weakening at the origin of unconventional singularity. a. Evolution of local shear stress τ, with slip velocity for one event. **b.** Temperature evolution with slip velocity at asperity scale compared with melting temperature of PMMA ($T_m = 160$). **c.** Slip dependence of breakdown work (curves are normalized respectively by G_c and D_c). W_{bd} evolution exhibits two power laws with exponents of ~2 and ~0.6. The experimental curves are all described by the asymptotic solutions related to an adiabatic regime for small D and a diffusive regime for large D. The dotted black line shows the expected evolution of W_{bd} assuming LEFM at the strain gauges position.